Dalton Transactions

ROYAL SOCIETY OF CHEMISTRY

PAPER

View Article Online
View Journal | View Issue

Check for updates

Cite this: *Dalton Trans.*, 2023, **52**, 2863

Ru(IV)–Ru(IV) complexes having the doubly oxido-bridged core with a bridging carbonato or hydrogencarbonato ligand†

Tomoyo Misawa-Suzuki * and Hirotaka Nagao *

Received 21st December 2022,
Accepted 1st February 2023

DOI: 10.1039/d2dt04080h

rsc.li/dalton

Ru(IV)–Ru(IV) complexes having the doubly oxido-bridged diamond core with a bridging carbonato or hydrogencarbonato ligand, $[\{Ru^{IV}(ebpma)\}_2(\mu\text{-}O)_2(\mu\text{-}O_2CO(H)_m)]X_n$ (ebpma; ethylbis(2-pyridylmethyl) amine, m = 0; **[IV,IV]**X_2 (X = PF_6, ClO_4), m = 1; **[IV,IV_1H]**$(ClO_4)_3$), were isolated *via* the oxidation of the corresponding carbonato-bridged Ru(III)–Ru(IV) complex ($[\mathbf{III,IV}]^+$), and "**[IV,IV]**$(ClO_4)_2$ and **[IV,IV_1H]** $(ClO_4)_3$" were structurally characterized. The electrochemical and spectroscopic properties of $[\mathbf{IV,IV}]^{2+}$ and $[\mathbf{IV,IV\_1H}]^{3+}$ were investigated both in organic solvents and aqueous solutions. The reactivity toward organic solvents having (a) methyl group(s) and reactions with organic substrates were studied as well. This should be the first time when systematic comparisons of the Ru(IV)–Ru(IV) species and corresponding Ru(III)–Ru(IV) complexes in the same tridentate ligand system were made.

Introduction

Singly and doubly oxido-bridged multi-nuclear transition metal complexes have been of interest as the reaction centers of oxidation reactions. For the oxidation of methane, the active site of the reaction mediator, soluble methane monooxygenase (sMMO), shows a wide range of oxidation states from Fe(II)–Fe(II) to Fe(IV)–Fe(IV), with the elaborate changes of the frameworks during the reaction.[1] Studies on the structural changes around the dinuclear oxido-bridged metal core accompanied by redox and protonation/deprotonation reactions are important for understanding the reaction mechanisms. A number of studies on the electronic structures, catalytic oxidation reactions and model reactions with sMMO analogues with diiron centers,[2] or some with dinickel centers[3] have been reported in homogeneous systems, which are not limited to the rich chemistry of mononuclear metal–oxido species by, *e.g.* the 8th group iron,[4] ruthenium,[5] and osmium[6] centers. However, reports on those with diruthenium centers are limited although, only recently, a light-driven methane monooxygenation with the dinuclear Ru(IV)–Ru(IV) complex was reported.[7]

In this sense, we have been investigating Ru(III)–Ru(IV) dimers having the $\{Ru_2(\mu\text{-}O(H))_2(\mu\text{-}O_2Y\text{–}Z)\}^{2+}$ (Y–Z = C–CH_3 (acetato), N═O(nitrato)) core.[8c,d] Instead of acetate, carbonate with a terminal oxygen, a potential site as a proton carrier site, was introduced as a bridging ligand.[8e] We have reported Ru(III)–Ru(IV) complexes with the doubly oxido- or hydroxido-bridged diamond core, $M[\{Ru^{III,IV}(L)\}_2(\mu\text{-}O)_2(\mu\text{-}O_2CO)]_2(PF_6)_3$ ($M[\mathbf{III,IV}]_2\text{-}(PF_6)_3$; M^+ = Na^+, K^+), $[\{Ru^{III,IV}(L)\}_2(\mu\text{-}O)_2(\mu\text{-}O_2COH)](PF_6)_2$ ($[\mathbf{III,IV\_1H}](PF_6)_2$), and $M[\{Ru^{III,IV}(L)\}_2(\mu\text{-}O)(\mu\text{-}OH)(\mu\text{-}O_2COH)](ClO_4)_4$ ($M[\mathbf{III,IV\_2H}](ClO_4)_4$; M^+ = Na^+, K^+), in which L is the tridentate ethylbis(2-pyridylmethyl)amine (ebpma) ligand.[8e] The reversible protonation/deprotonation reactions, crystal structures, and electronic structures have been discussed.

It is worth studying the fixation of hydrogencarbonate (HCO_3^-) on the transition metal center(s) as well as carbonate (CO_3^{2-}) fixation for the evaluation of its activity using transition metal complexes. HCO_3^- exists in an equilibrium mixture of CO_3^{2-} and H_2CO_3 (CO_2 (aq.)) depending on pH. Thus, carbonate easily undergoes protonation, resulting in decarboxylation under acidic conditions ($CO_3^{2-} + 2H^+ \rightleftarrows CO_2 + H_2O$). Isolation of hydrogencarbonato-bound transition metal complexes has been attempted in the monodentate coordination (*e.g.* $\{Ni^I\text{–}OC(O)OH\}$,[9] $\{Zn^{II}\text{–}OC(O)OH\}$[10]) or in the bidentate coordination through its two oxygen atoms (*e.g.* $\{Mo_2^{IV,IV}(\mu\text{-}O_2COH)\}$,[11] $\{Ru_2^{I,I}(\mu\text{-}O_2COH)\}$[12] or $\{Rh_2^{IV,IV}(\mu\text{-}O_2COH)\}$[13]). However, no one has isolated HCO_3^--bound transition metal complexes with both the Ru(IV)–Ru(IV) and Ru(III)–Ru(IV) centers, in which ancillary ligands are the same.

In this report, Ru(IV)–Ru(IV) complexes with the metal–oxido diamond core, $[\{Ru^{IV,IV}(ebpma)\}_2(\mu\text{-}O)_2(\mu\text{-}O_2CO)](X)_2\cdot nH_2O$ ($[\mathbf{IV,IV}](X)_2\cdot nH_2O$, X = PF_6, ClO_4) and $[\{Ru^{IV,IV}(ebpma)\}_2(\mu\text{-}O)_2(\mu\text{-}$

Department of Materials and Life Sciences, Faculty of Science and Technology, Sophia University, 7-1 Kioicho Chiyoda-ku, Tokyo 102-8554, Japan.
E-mail: t_misawa@sophia.ac.jp

†Electronic supplementary information (ESI) available. CCDC 2115482 and 2115484. For ESI and crystallographic data in CIF or other electronic format see DOI: https://doi.org/10.1039/d2dt04080h

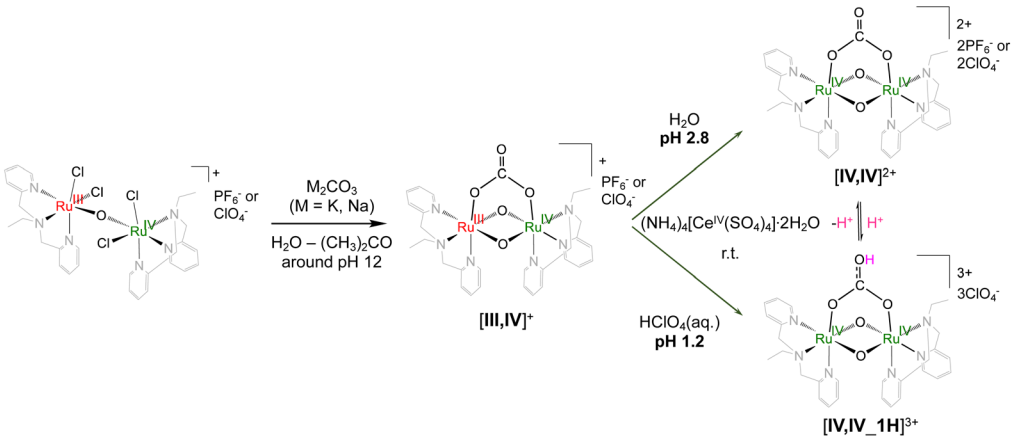

Scheme 1 Synthesis of Ru(IV)–Ru(IV) complexes having carbonato and hydrogencarbonato bidentate ligands.

$O_2COH)](ClO_4)_3{\cdot}HClO_4{\cdot}7H_2O$ ([**IV,IV_1H**]$(ClO_4)_3{\cdot}HClO_4{\cdot}7H_2O$), were isolated (Scheme 1) and structurally characterized by X-ray crystallography. Although there are a few studies on the Ru(IV)–Ru(IV) complexes with the singly,[14] doubly[15] or triply[16] oxido-bridged core, the study on Ru(IV)–Ru(IV) complexes with the $\{Ru_2(\mu\text{-}O)_2(\mu\text{-}O_2Y\text{–}Z)\}$ framework should be the first report, to the best of our knowledge. The direct comparisons of the electronic structures and electrochemical and spectroscopic properties with those of the corresponding Ru(III)–Ru(IV) complexes in acetonitrile were achieved. The report on electrochemical and spectroscopic behaviors of $[\mathbf{III,IV\_1H}]^{2+}$ or $[\mathbf{III,IV\_2H}]^{3+}$ in acetonitrile is also the first report beyond those in aqueous solutions. The reactions of $[\mathbf{IV,IV}]^{2+}$ and $[\mathbf{IV,IV\_1H}]^{3+}$ in solvents and in the presence of organic substrates were studied to gain mechanistic insights.

Results and discussion

Syntheses and electronic structures

The perchlorate salts of $[\mathbf{IV,IV}]^{2+}$ and $[\mathbf{IV,IV\_1H}]^{3+}$ were isolated *via* the one-electron oxidation of Na[**III,IV**]$_2(ClO_4)_3{\cdot}17H_2O$ in water with an equimolar amount of $(NH_4)_4[Ce^{IV}(SO_4)_4]{\cdot}2H_2O$ (CAS) at pH 2.8 and pH 1.2, respectively, at room temperature. The pH value was adjusted by using perchloric acid solutions for the formation of $[\mathbf{IV,IV\_1H}]^{3+}$, in which one-protonation to the uncoordinated terminal oxygen of the carbonato ligand occurred after one-electron oxidation of the $\{Ru_2^{III,IV}(\mu\text{-}O)_2\}$ core (Scheme 1). The pK_a value of $[\mathbf{IV,IV\_1H}]^{3+}$ was determined as 1.1 by spectroscopic studies in aqueous solution (Fig. S2, S3 and Table S1†). Since the cationic character was higher for the Ru(IV)–Ru(IV) core, the pK_a value was lower than that of the corresponding Ru(III)–Ru(IV) complex, $[\mathbf{III,IV\_1H}]^{2+}$ (pK_a; 3.9).[8e] The spectroscopic studies in aqueous solutions revealed that a further one-protonated species, $\{[\mathbf{IV,IV\_2H}]^{4+}\}$, could exist at pH lower than 0.6. Although the isolation of $\{[\mathbf{IV,IV\_2H}]^{4+}\}$ was attempted a couple of times, we had difficulties in reproducibility.

$[\mathbf{IV,IV}](ClO_4)_2$ and $[\mathbf{IV,IV\_1H}](ClO_4)_3$ showed the effective magnetic moments (μ_{eff}) of 1.04μ_B and 0.85μ_B at 298 K, indicating that although the antiferromagnetic coupling of the two paramagnetic d^4 centers is observed, paramagnetic characters are maintained. The paramagnetic characters prevented us from fully understanding the ^{1}H NMR signals although they were observed within the range of 0–12 ppm (Fig. S1†). In the IR spectra, the characteristic absorption band attributed to ν_{as}(CO) was observed at 1570(s) cm^{-1} for $[\mathbf{IV,IV}](ClO_4)_2{\cdot}2H_2O$ and 1591(s) cm^{-1} for $[\mathbf{IV,IV}](PF_6)_2{\cdot}1.5H_2O$ (Fig. S7†), which were 70–90 cm^{-1} higher than that of M[**III,IV**]$_2(PF_6)_3$.[8e] The difference is originating from the more cationic character of the Ru(IV)–Ru(IV) centers, resulting in the stronger Ru(IV)–O(carbonato) bond, weaker bondings of the O–C–O moiety, and stronger C=O bond. Also, the absence of M^+ in the vicinity of $[\mathbf{IV,IV}]^{2+}$, although it was observed for $[\mathbf{III,IV}]^+$, might have some effects on the larger value for $[\mathbf{IV,IV}]^{2+}$. For [**IV,IV_1H**]$(ClO_4)_3$, ν_{as}(CO) was observed at 1437 cm^{-1} (Fig. S7†), which is consistent with that of [**III,IV_1H**]$(PF_6)_2$ (1437 cm^{-1}),[8e] owing to the more delocalized electronic structure over the O–C(OH)–O moiety.

Single crystal X-ray crystallography

By X-ray crystallographic analyses of $[\mathbf{IV,IV}]^{2+}$ and $[\mathbf{IV,IV\_1H}]^{3+}$, (Fig. 1, S18 and Tables 1, S4 and S5†), each ruthenium center is coordinated with tridentate ebpma in a *facial* manner, the bridging oxido or hydroxido ligands, and one of the oxygen atoms of the bridging carbonato or hydrogencarbonato ligand. Along with the complex cations, two or three ClO_4^- were co-crystalized with $[\mathbf{IV,IV}]^{2+}$ or $[\mathbf{IV,IV\_1H}]^{3+}$, respectively, revealing that they surely have the Ru(IV)–Ru(IV) centers. The asymmetric unit of $[\mathbf{IV,IV\_1H}]^{3+}$ (Fig. 1) contained one solvent water molecule in the vicinity of the terminal OH group of hydrogencarbonato, forming the hydrogen bond network with the perchlorate oxygen atoms. The perchlorate near $[\mathbf{IV,IV\_1H}]^{3+}$ was neutral $HClO_4$, revealed by one elongated Cl–O length. Thus, the whole chemical formula of $[\mathbf{IV,IV\_1H}]^{3+}$ should be denoted as [**IV,IV_1H**]$(ClO_4)_3{\cdot}HClO_4{\cdot}H_2O$. The Ru–O(oxido) lengths in

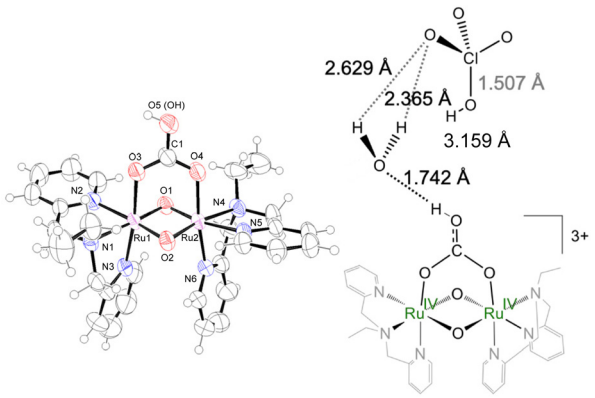

Fig. 1 Crystal structure of [**IV,IV_1H**]$^{3+}$ shown at the 50% probability level (left) and the hydrogen bonding network (right).

[**IV,IV**]$^{2+}$and [**IV,IV_1H**]$^{3+}$ are closer to each other and comparable to those of the doubly oxido-bridged complexes in the Ru(IV)–Ru(IV) state, $[\{Ru^{IV,IV}(OH_m)(L')\}_2(\mu\text{-}O)_2]^{n+}$ (L′; $[(\eta^5\text{-}C_5H_5)Co(C_2H_5O)_2P{=}O_3]^-$) (1.893(4)–1.926(4) Å),[15a] whereas shorter by 0.03–0.05 Å than the $Ru^{3.5}$–O lengths in both [**III,IV_1H**]$^{2+}$ and Na[**III,IV_2H**]$^{3+}$,[8e] and by 0.1 Å shorter than the $Ru^{3.5}$–OH lengths in Na[**III,IV_2H**]$^{3+}$ (ave. 2.021 Å).[8e] The Ru···Ru distances (2.4261(3) and 2.4389(3) Å) are shorter than those in $[\{Ru^{IV,IV}(OH_m)(L')\}_2(\mu\text{-}O)_2]^{m+}$ (2.452(1)–2.505(4) Å)[15a] due to the difference in the framework. The Ru···Ru distances show that there is the dπ(Ru)–dπ(Ru) interaction in addition to the six-coordinate environment around the Ru centers. The shapes of the diamond core of [**IV,IV**]$^{2+}$ and [**IV,IV_1H**]$^{3+}$ are different from $[\{Ru^{IV,IV}(OH_n)(L')\}_2(\mu\text{-}O)_2]^{m+}$,[15a] because of the coordination of the bidentate (hydrogen)carbonato ligand on the $\{Ru_2(\mu\text{-}O)_2\}$ core. The O–O(H) distances are longer for the core with (i) the lower oxidation state of Ru, (ii) the hydroxido bridge rather than the oxido bridge, and (iii) HCO_3^- over CO_3^{2-}; [**III,IV_2H**]$^{3+}$ (3.058 Å) > [**III,IV**]$^+$ (3.026 Å) > [**III,IV_1H**]$^{3+}$ (2.994 Å) > [**IV,IV**]$^{2+}$ (2.949 Å) > [**IV,IV_1H**]$^{3+}$ (2.934 Å). The Ru···Ru distance (Å) is longer simply in the order of lower oxidation states of the Ru centers and with weaker σ-donating oxygen; [**III,IV_2H**]$^{3+}$ (2.533 Å)[8e] > [**III,IV_1H**]$^{2+}$ (2.454 Å)[8e] > [**III,IV**]$^+$ (2.443 Å)[8e] > [**IV,IV_1H**]$^{3+}$ (2.439 Å) > [**IV,IV**]$^{2+}$ (2.426 Å).

The Ru–N(amine) lengths were unambiguously influenced by the number of protons on the carbonato and oxido ligands, and the electronic state of the Ru centers; [**III,IV**]$^+$ (ave. 2.182 Å)[8e] > [**III,IV_1H**]$^{2+}$ (ave. 2.157 Å)[8e] > [**IV,IV**]$^{2+}$ (ave. 2.147 Å) > [**IV,IV_1H**]$^{3+}$ ≈ Na[**III,IV_2H**]$^{3+}$ (ave. 2.131 Å).[8e] Carbonato is more σ-donating than hydrogencarbonato that makes the Ru–N(amine, σ-donor) lengths longer. Due to protonation to the oxido ligand, the basicity of oxygen became lower and, accordingly, the σ-donating N(amine) atom which located at the *trans* position to the oxido ligand was bound more strongly to the Ru centers. The C=O length of [**IV,IV**]$^{2+}$ is shorter by 0.025 Å than that of [**III,IV**]$^+$, which is consistent with the higher wavenumber of ν_{as}(CO) for [**IV,IV**]$^{2+}$. The metric parameters around hydrogencarbonato of [**IV,IV_1H**]$^{3+}$ are in agreement with those in [**III,IV_1H**]$^{2+}$ [8e] and Na[**III,IV_2H**]$^{3+}$ [8e] (Table 1).

UV-vis-NIR spectroscopy in acetonitrile

The UV-vis-NIR absorption spectra of [**IV,IV**]$^{2+}$ and [**IV,IV_1H**]$^{3+}$ exhibited relatively weak and broad bands at 762 and 669 nm, and furthermore, much weaker and broader bands were also found at around 1000 and 1100 nm in CH_3CN at 25 °C (Fig. S4†). Similar absorption bands at 632–694 nm and around 1070 nm have been reported for the diruthenium complexes having the $\{Ru_2^{IV,IV}(\mu\text{-}O)_2\}$ core.[17] The spectroscopic parameters in CH_3CN are listed in Tables 2 and S1† with the electrochemical information. In comparison with [**III,IV**]$^+$ (1067 nm)[8e] and [**III,IV_1H**]$^{2+}$ (972 nm) (Fig. S5†), or the corresponding acetato- or nitrato-bridged complexes ($[\{Ru^{III,IV}(ebpma)\}_2(\mu\text{-}O)_2(\mu\text{-}O_2Y\text{–}Z)]^{2+}$; Y–Z = C–$CH_3$, [**III,IV**$(CH_3CO_2)]^{2+}$ or N=O, [**III,IV**$(NO_3)]^{2+}$) at 977 or 762 nm (Fig. S6†),[8c] the characteristic broad bands were observed at shorter wavelengths, indicating that the energy difference of the MOs of the $\{Ru_2^{IV,IV}(\mu\text{-}O)_2\}$ core becomes higher than those of the $\{Ru_2^{III,IV}(\mu\text{-}O)_2\}$ core. We could also conclude that the $\{Ru_2(\mu\text{-}O)_2\}$–$\{Ru_2(\mu\text{-}O)_2\}^*$ transition energies are higher and the intensities (ε/M^{-1} cm^{-1}) are stronger for the HCO_3^--bound complexes, [**IV,IV_1H**]$^{3+}$ or [**III,IV_1H**]$^{2+}$, than for the CO_3^{2-}-bound ones, [**IV,IV**]$^{2+}$ or [**III,IV**]$^+$, respectively. Comparing the corresponding absorption bands of the Ru(IV)–Ru(IV) species prepared through electrochemical one-electron oxidation of

Table 1 Comparisons of bond lengths/Å of Ru(IV)–Ru(IV) with those of Ru(III)–Ru(IV)[8e] complexes

	[**IV,IV**]$(ClO_4)_2$·$2H_2O$		[**IV,IV_1H**]$(ClO_4)_3$·$HClO_4$·H_2O		K[**III,IV**]$_2(PF_6)_3$·$3CH_3CN$·$4H_2O$[8e]		[**III,IV_1H**]$(ClO_4)_2$·H_2O[8e]		Na[**III,IV_2H**]$(ClO_4)_4$·$4H_2O$[8e]	
Ru1,2–O1	1.905(3)	1.914(3)	1.918(2)	1.899(2)	1.940(5)	1.940(4)	1.9372(18)	1.9329(17)	1.954(4)	1.953(4)
Ru1,2–O2	1.904(3)	1.919(3)	1.902(2)	1.914(2)	1.938(4)	1.962(5)	1.9360(18)	1.9387(18)	2.022(4)	2.019(3)
Ru1···Ru2	2.4261(3)		2.4389(3)		2.4434(8)		2.4547(2)		2.5332(5)	
O1···O2	2.949		2.934		3.026		2.994		3.058	
Ru–O3,4	2.031(3)	2.022(3)	2.069(2)	2.065(2)	2.055(4)	2.063(4)	2.0799(17)	2.0968(18)	2.078(4)	2.083(4)
Ru–N1,4	2.147(3)	2.146(3)	2.130(3)	2.134(3)	2.195(5)	2.168(5)	2.158(2)	2.156(2)	2.131(4)	2.123(4)
Ru–N2,5	2.091(3)	2.091(3)	2.078(3)	2.086(3)	2.113(7)	2.100(6)	2.087(2)	2.093(2)	2.072(3)	2.088(4)
Ru–N3,6	2.076(3)	2.072(3)	2.047(3)	2.056(3)	2.061(5)	2.057(5)	2.039(2)	2.042(2)	2.042(5)	2.045(5)
O3,4–C29	1.311(5)	1.312(4)	1.265(4)	1.269(4)	1.309(8)	1.301(8)	1.258(3)	1.266(3)	1.266(7)	1.266(6)
C29–O5	1.228(5)		1.297(4)		1.252(7)		1.315(3)		1.313(7)	

Table 2 Spectroscopic parameters and redox potentials of the Ru(IV)–Ru(IV) and Ru(III)–Ru(IV) complexes in acetonitrile

λ (ε)/nm (M^{-1} cm^{-1}) in acetonitrile $\{Ru_2(\mu\text{-}O)_2\}$–$\{Ru_2(\mu\text{-}O)_2\}$[a]				$E_{1/2}$/V (*vs.* $Ag/AgNO_3$) Ru(IV)–Ru(IV)/Ru(III)–Ru(IV)
$[\mathbf{IV,IV}]^{2+}$	762 (1440)	$[\mathbf{III,IV}]^{+}$	1067 (660)[8e]	0.15
$[\mathbf{IV,IV\_1H}]^{3+}$	669 (1970)	$[\mathbf{III,IV\_1H}]^{2+}$	972 (1490)	0.60
—		$[\mathbf{III,IV\_2H}]^{3+}$	964 (1330)	1.32
$[\mathbf{IV,IV}(CH_3CO_2)]^{3+}$	677 (—)	$[\mathbf{III,IV}(CH_3CO_2)]^{2+}$	977 (1440)[8c]	0.57[8c]
—		$[\mathbf{III,IV}(CH_3CO_2)]^{3+}$ [a]	1187 (320)[8d]	1.33[8d]
$[\mathbf{IV,IV}(NO_3)]^{3+}$	586 (—)	$[\mathbf{III,IV}(NO_3)]^{2+}$	762 (1300)[8c]	0.93[8c]

[a] $\{Ru_2(\mu\text{-}O)(\mu\text{-}OH)\}$ core.

$[\mathbf{III,IV}(CH_3CO_2)]^{2+}$ and $[\mathbf{III,IV}(NO_3)]^{2+}$, namely, $[\mathbf{IV,IV}(CH_3CO_2)]^{3+}$ (677 nm) and $[\mathbf{IV,IV}(NO_3)]^{3+}$ (586 nm),[8c] good correlations between the redox potentials and the absorption wavelengths are found (Table 2).

Electrochemistry in acetonitrile

Cyclic voltammograms (CVs) show a reversible reduction wave at 0.15 V for $[\mathbf{IV,IV}]^{2+}$ or 0.60 V ($E_{1/2}$ *vs.* Ag|0.01 M $AgNO_3$) for $[\mathbf{IV,IV\_1H}]^{3+}$ in acetonitrile at 25 °C (Fig. S8†), which is assigned to the one-electron process between Ru(IV)–Ru(IV) and Ru(III)–Ru(IV) (Fig. S9, S13 and Tables S2, S3†). Hydrodynamic voltammetry (HDV) also supports the electronic state of Ru(IV)–Ru(IV) for $[\mathbf{IV,IV}]^{2+}$ and $[\mathbf{IV,IV\_1H}]^{3+}$, by comparing the rest potentials with those of $\{Na^+ + [\mathbf{III,IV}]^+\}$ and $[\mathbf{III,IV\_1H}]^{2+}$ (Fig. S10–S12 and S14–S16†). The one-electron oxidation process from $[\mathbf{III,IV\_2H}]^{3+}$ to $[\mathbf{IV,IV\_2H}]^{4+}$ was observed at 1.32 V (E_{pa}) as an irreversible process. Through one-protonation to the uncoordinated oxygen of carbonato, which locates far from the $\{Ru_2(\mu\text{-}O)_2\}$ core, the redox potential shifted by +0.45 V and upon an additional one-protonation to the oxido ligand on the diamond core $\{Ru_2(\mu\text{-}O)_2\}$, the potential shifted further by as much as +0.72 V. The differences in the effects of protonation to the $\{Ru_2(\mu\text{-}O)_2\}$ core or away from the core on the redox potentials were revealed. This must be the first discussion ever had, because even in our previous report on $[\mathbf{III,IV}(CH_3CO_2)]^{2+}$, and only the effect of one-protonation to one of the bridging oxido ligands of the $\{Ru_2(\mu\text{-}O)_2\}$ core (by +0.76 V) has been discussed.[8d] The one-electron redox reactions should occur at the $\{Ru_2(\mu\text{-}O)_2\}$ core, which was supported by theoretical calculations[18] that revealed the SOMO delocalization mainly over the $\{Ru_2(\mu\text{-}O)_2\}$ core of both $[\mathbf{IV,IV}]^{2+}$ (Fig. S51 and Table S8†) and $[\mathbf{IV,IV\_1H}]^{3+}$ (Fig. S52 and Table S9†), with a little contribution from the carbonato or hydrogencarbonato oxygen.

As the one-electron redox potentials between Ru(IV)–Ru(IV) and Ru(III)–Ru(IV) become higher in the order of $[\mathbf{III,IV}(NO_3)]^{2+}$ (0.93 V) > $[\mathbf{III,IV\_1H}]^{2+}$ (0.60 V) ≈ $[\mathbf{III,IV\_(CH_3CO_2)}]^{2+}$ (0.57 V) > $[\mathbf{III,IV}]^{+}$ (0.15 V), the $\{Ru_2(\mu\text{-}O)_2\}$–$\{Ru_2(\mu\text{-}O)_2\}$* transition energies become higher in the same order, owing to the greater stabilization of the $\{Ru_2(\mu\text{-}O)_2\}$ core (SOMO).

UV-vis-NIR spectroscopy and electrochemistry in water

In aqueous solutions containing $HClO_4$(aq) and NaOH(aq), the spectroscopic properties were studied as a function of pH (Fig. S2 and Table S1†). Between pH 1.25 and 5.23, where $[\mathbf{IV,IV}]^{2+}$ should be present, λ_{max} of the characteristic band, that was assigned to the transitions on the $\{Ru_2(\mu\text{-}O)_2\}$ core, was observed at 704 ± 4 nm within the apparatus resolution. The weaker band in the NIR region was observed as well at around 1090–1100 nm. The effects of water on $[\mathbf{IV,IV}]^{2+}$ seemed quite large since the differences in λ_{max} were by as much as 25–70 nm compared to those in organic solvents (729–776 nm). Accordingly, the brown colored complex $[\mathbf{IV,IV}]^{2+}$ readily changed into emerald-green in aqueous solution. At pH 0.88, λ_{max} was observed at 700 nm, corresponding to $[\mathbf{IV,IV\_1H}]^{3+}$; however at pH 0.55, one more proton addition to $[\mathbf{IV,IV\_1H}]^{3+}$ seemed to occur since the λ_{max} shifted by 10 nm to 681 nm. We believe that $\{[\mathbf{IV,IV\_2H}]^{4+}\}$ could be present in solution without decarboxylation even under such harsh acidic conditions, although it was not isolated.

The CPET processes were observed in the CVs in aqueous solutions at different pH values (Fig. S17,† shown *vs.* Ag|AgCl); at pH 2.7, 0.39 V (*vs.* $Ag|Ag^+$) for a $1e^-/1H^+$ process of $[\mathbf{III,IV\_1H}]^{2+}/[\mathbf{IV,IV}]^{2+}$ (eqn (2)), at pH 1.8, 0.44 V for a $1e^-/2H^+$ process of $[\mathbf{III,IV\_2H}]^{3+}/[\mathbf{IV,IV}]^{2+}$ (eqn (3)) and at pH 1.1, 0.53 V for a $1e^-/1H^+$ process of $[\mathbf{III,IV\_2H}]^{3+}/[\mathbf{IV,IV\_1H}]^{3+}$ (eqn (6)). Above pH 4, the redox potentials between Ru(IV)–Ru(IV) and Ru(III)–Ru(IV) were similar, and thus one-electron transfer without proton transfer occurred between $[\mathbf{IV,IV}]^{2+}$ and $[\mathbf{III,IV}]^{+}$ (eqn (1)).

$$[\mathbf{IV,IV}]^{2+} + e^- \rightarrow [\mathbf{III,IV}]^{+} \quad (1)$$

$$[\mathbf{IV,IV}]^{2+} + e^- + H^+ \rightarrow [\mathbf{III,IV\_1H}]^{2+} \quad (2)$$

$$[\mathbf{IV,IV}]^{2+} + e^- + 2H^+ \rightarrow [\mathbf{III,IV\_2H}]^{3+} \quad (3)$$

$$[\mathbf{IV,IV\_1H}]^{3+} \rightarrow [\mathbf{IV,IV}]^{2+} + H^+ \quad (4)$$

$$[\mathbf{IV,IV\_1H}]^{3+} + e^- \rightarrow [\mathbf{III,IV\_1H}]^{2+} \quad (5)$$

$$[\mathbf{IV,IV\_1H}]^{3+} + e^- + H^+ \rightarrow [\mathbf{III,IV\_2H}]^{3+} \quad (6)$$

$$[\mathbf{IV,IV\_1H}]^{3+} + e^- + 2H^+ \rightarrow \{[\mathbf{III,IV\_3H}]^{4+}\}* \quad (7)$$

*$\{[\mathbf{III,IV\_3H}]^{4+}\}$ has not been isolated and characterized.

Spectroscopic studies on the reactions in various solvents and with substrates

The solvent dependency of UV-vis-NIR spectroscopic behaviors was also of interest. However, both $[\mathbf{IV,IV}]^{2+}$ and $[\mathbf{IV,IV\_1H}]^{3+}$ were more reactive than to evaluate the spectroscopic properties at 25 °C. The spectroscopic data regarding the reactions are listed in Tables 3 and S6.† Although some of them showed a relationship between BDE_{C-H} of the solvent and the k_{obs} value (*e.g.* between acetone and acetonitrile), others did not (*e.g.* between methanol and DMSO), and thus some more factors for the reaction rates might be considered.

Upon dissolution of $[\mathbf{IV,IV\_1H}]^{3+}$ in dehydrated DMSO (Fig. S19†) and methanol (Fig. 2), the proton at hydrogencarbonato of $[\mathbf{IV,IV\_1H}]^{3+}$ was dissociated (eqn (4)), and then $1e^-/2H^+$ transfer to $[\mathbf{IV,IV}]^{2+}$ proceeded showing isosbestic points, affording $[\mathbf{III,IV\_2H}]^{3+}$ quantitatively (eqn (3)). In nitromethane, the $1e^-$ transfer to $[\mathbf{IV,IV\_1H}]^{3+}$ proceeded to change into $[\mathbf{III,IV\_1H}]^{2+}$ (eqn (5), Fig. S20†). In acetone or acetonitrile, $1e^-$ transfer (eqn 5) or CPET ($1e/1H^+$ or $1e^-/2H^+$ transfer) occurred to $[\mathbf{IV,IV}]^{2+}$ and $[\mathbf{IV,IV\_1H}]^{3+}$ (eqn (2), (3), (6) and (7)).

The reactions of $[\mathbf{IV,IV}]^{2+}$ in acetone proceeded with isosbestic points, forming only $[\mathbf{III,IV\_2H}]^{3+}$ through the $1e^-/2H^+$ transfer (eqn (3), Fig. S26†). The k_{obs} values were analyzed as the pseudo first-order reaction and the rate constants (k_{obs}, s^{-1}) were investigated at different complex concentrations (Fig. S26–S28†). $[\mathbf{IV,IV}]^{2+}$ was quantitatively changed into $[\mathbf{III,IV\_2H}]^{3+}$ by $1e^-/2H^+$ transfer (eqn (3)) and k_{obs} was not related to the $[\mathbf{IV,IV}]^{2+}$ concentration (Fig. S29†). In the case of $[\mathbf{IV,IV\_1H}]^{3+}$, different reactions occurred depending on the complex concentration (lower/higher than 0.2 mM) (Fig. 2, S30 and S33†). The k_{obs} value was analyzed by two-step first-order linear approximations and the reaction rates were in a linear and negative relationship with the concentration of $[\mathbf{IV,IV\_1H}]^{3+}$ (Fig. S33†). The reaction rates were higher below 0.2 mM, where the reaction product was $[\mathbf{III,IV\_2H}]^{3+}$ *via* $1e^-/1H^+$ transfer (eqn (6)), and slower above 0.2 mM, where only $[\mathbf{III,IV\_1H}]^{2+}$ was formed *via* $1e^-$ transfer (eqn (5)).

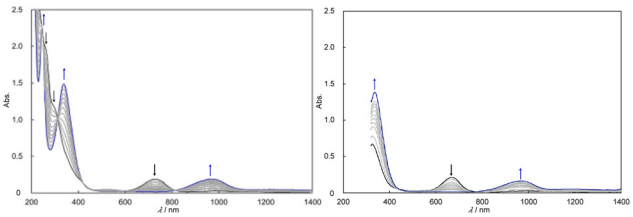

Fig. 2 Spectral changes of $[\mathbf{IV,IV\_1H}]^{3+}$ (0.13 mM) into $[\mathbf{III,IV\_1H}]^{2+}$ *via* the formation of $[\mathbf{IV,IV}]^{2+}$ in dehydrated methanol (left) and those directly into $[\mathbf{III,IV\_1H}]^{2+}$ in acetone (right) under air at 25 °C.

The kinetic isotopic effect (KIE, divided by the number of equivalent active hydrogen atoms) was observed in acetone-d_6 for both $[\mathbf{IV,IV}]^{2+}$ (5.1) (Fig. S28†) and $[\mathbf{IV,IV\_1H}]^{3+}$ (2.2–24) (Fig. S32†) as summarized in Table S6.† Hydrogen atom abstraction (HAA) of acetone should be involved. However, because they are stoichiometric reactions and the concentration of product(s) is rather low, the analysis of each reaction product was demanding.

The effects of water content in acetone on the reaction rates were observed as well. The reaction rates (k_{obs}, h^{-1}) of $[\mathbf{IV,IV}]^{2+}$ in 99.5% acetone were a little larger than those in dehydrated acetone (Fig. S27†). The reaction rates of $[\mathbf{IV,IV\_1H}]^{3+}$ in 99.5% acetone were 0.50 (initial) and 0.29 (following) (Fig. S30vi†)

Table 3 Spectroscopic investigations on the reactivity of $[\mathbf{IV,IV}]^{2+}$ and $[\mathbf{IV,IV\_1H}]^{3+}$ in solution

	Before reaction		After reaction		
Solv.[a]	Complex	λ_{max}/nm	Product	λ_{max}/nm	k_{obs}, h^{-1} at 0.13 mM, unless otherwise noted
DMSO (dehydrated)	$[\mathbf{IV,IV\_1H}]^{3+}$ → $[\mathbf{IV,IV}]^{2+}$ [b]	756	$[\mathbf{III,IV\_2H}]^{3+}$	341, 965 (342, 966)[c]	0.135 (initial) 0.039 (following)
Methanol (dehydrated)	$[\mathbf{IV,IV\_1H}]^{3+}$ → $[\mathbf{IV,IV}]^{2+}$ [b]	729	$[\mathbf{III,IV\_2H}]^{3+}$	338, 966 (337, 970)[c]	2.3
Acetone (dehydrated)	$[\mathbf{IV,IV}]^{2+}$	776	$[\mathbf{III,IV\_2H}]^{3+}$	965 (967)[c]	0.22 (0.14 mM)
Acetone		773	$[\mathbf{III,IV\_2H}]^{3+}$	962–963 (967)[c]	0.27 (0.20 mM)
Acetonitrile		762	$[\mathbf{III,IV\_2H}]^{3+}$	959 (964)[c]	0.043 (0.20 mM)
pH 4 water ($HClO_4$–NaOH)		705	$[\mathbf{III,IV}]^{+}$	335, ~1028 (337, 1035)[d]	—
Acetone (dehydrated)	$[\mathbf{IV,IV\_1H}]^{3+}$	666	$[\mathbf{III,IV\_2H}]^{3+}$	964 (967)[c]	0.14 (initial) 0.013 (following)
Acetone		665	$[\mathbf{III,IV\_1H}]^{2+}$; >0.2 mM	974–977 (~973)[c]	0.40 (initial)
			$[\mathbf{III,IV\_2H}]^{3+}$; <0.2 mM	964–965 (967)[c]	0.22 (following)
Acetonitrile		670	$[\mathbf{III,IV\_2H}]^{3+}$	963 (964)[c]	0.0019 (0.30 mM)
Nitromethane		674	$[\mathbf{III,IV\_1H}]^{2+}$	962 (966)[c]	0.0039
pH 1.1 water ($HClO_4$–NaOH)		697	$[\mathbf{III,IV\_2H}]^{3+}$	~293, ~1180 (~298, 1170)[d]	—

[a] $BDEs_{C-H}$ (kcal mol^{-1});[19] DMSO 94, CH_3OH 96.06, $(CH_3)_2CO$ 96.0, and CH_3CN 97.0. [b] Immediately deprotonated upon dissolution. [c] The spectra of authentic samples are shown in Fig. S4 (acetonitrile), S21 (methanol), S22 (DMSO), S23 (nitromethane) and S34 (acetone).† [d] The data of authentic samples of pH 6.3 and 1.0 aqueous solutions are from ref. 8*e* and also shown in Table S1.†

and those in dehydrated acetone–D_2O (v/v = 99.5/0.5) were 0.39 and 0.21, whereas 0.14 and 0.013 in dehydrated acetone (Fig. S31†). These results revealed that the KIE due to the D–O cleavage of D_2O was hardly observed and the C–H activation of acetone could possibly occur. For comparisons, the reactivity was evaluated in water as well. In pH 4 water, $[\mathbf{IV,IV}]^{2+}$ showed a decay into $[\mathbf{III,IV}]^{+}$ by $1e^-$ transfer (eqn (1), Fig. S24†), which was different from the reactions in organic solvents. In pH 1 water, $[\mathbf{IV,IV\_1H}]^{3+}$ was changed into $[\mathbf{III,IV\_2H}]^{2+}$ through the $1e^-/1H^+$ transfer (eqn (6), Fig. S25†).

In acetonitrile, the reaction rates were much slower than those in acetone. $[\mathbf{IV,IV}]^{2+}$ underwent $1e^-/2H^+$ transfer to quantitatively give $[\mathbf{III,IV\_2H}]^{2+}$ (eqn (3), Fig. S35†). The reaction in acetonitrile-d_3 was performed for the 0.82 mM solution of $[\mathbf{IV,IV}]^{2+}$ and the KIE was 1.5 for the initial reaction, which lasted only for a moment, and 1.2 for the following reaction (Fig. S35†). Therefore, HAA of acetonitrile might be involved in the reactions of $[\mathbf{IV,IV}]^{2+}$. $[\mathbf{IV,IV\_1H}]^{3+}$ showed much lower reactivity than $[\mathbf{IV,IV}]^{2+}$, taking over a month to complete the reactions.

Then, in dehydrated acetonitrile, the oxidation reactions of cyclic organic compounds, benzyl alcohol, cyclohexene, cumene and ethylbenzene were studied. Based on the pK_a values and redox potentials (Scheme 2) of $[\mathbf{IV,IV}]^{2+}$ and $[\mathbf{IV,IV\_1H}]^{3+}$, the hydrogen accepting ability or BDE_{C-H} was calculated to be 84.3 and 92.7 kcal mol^{-1}, respectively, according to eqn (8).[20]

$$\mathrm{BDE\ (kcal\ mol^{-1})} = 1.37(\mathrm{p}K_a) + 23.06E_{1/2} + C_H \quad (8)$$

The dependency of the reaction rate on the concentration of the substrate (0.05–0.2 M) was studied. All could be analysed as the first-order linear relationships (k_{obs}, s^{-1}) and the second-order rate constants (k, M^{-1} s^{-1}) were evaluated (Fig. S37–S50, Table S7†). For the reactions with ethylbenzene, only those of $[\mathbf{IV,IV}]^{2+}$ were investigated since the reaction rates of $[\mathbf{IV,IV\_1H}]^{3+}$ were too slow to discuss at 25 °C. Independent of the kind of substrate, $[\mathbf{IV,IV}]^{2+}$ underwent $1e^-/2H^+$ transfer to form $[\mathbf{III,IV\_2H}]^{3+}$ (eqn 3) and $[\mathbf{IV,IV\_1H}]^{3+}$ changed solely into $\{[\mathbf{III,IV\_3H}]^{4+}\}^*$ (eqn (7)) or into a mixture of $\{[\mathbf{III,IV\_3H}]^{4+}\}^*$ and $[\mathbf{III,IV\_2H}]^{3+}$ (eqn (6) and (7)), where $\{[\mathbf{III,IV\_3H}]^{4+}\}^*$ seemed to be a transient intermediate that we have not identified. The reaction rates of $1e^-/2H^+$ transfer to $[\mathbf{IV,IV}]^{2+}$ to form $[\mathbf{III,IV\_2H}]^{3+}$ (eqn 3) (Fig. S38, S42, S46 and S50†) were greater than those of $1e^-/1H^+$ or $1e^-/2H^+$ transfer to $[\mathbf{IV,IV\_1H}]^{3+}$ (Fig. S40, S44 and S48†) (Table S7†), although BDE_{C-H} of $[\mathbf{IV,IV}]^{2+}$ is smaller than that of $[\mathbf{IV,IV\_1H}]^{3+}$. These results indicated that the uncoordinated terminal oxygen of carbonato in $[\mathbf{IV,IV}]^{2+}$ would better function as a one-proton acceptor than the oxido ligand(s). Although the plot of log(k', M^{-1} s^{-1}) against BDE was drawn based on the Bell–Evans–Polanyi equation (eqn (9)),[21] the relationships were not understandable, indicating that multiple reaction mechanisms are involved depending on the substrate.

$$\log k = \alpha\Delta H^\circ + C \quad (9)$$

Reactions with deuterated reagents, benzyl alcohol-d_2 (BA-d_2; $C_6H_5CD_2OH$, Fig. S37iv and S39iii†) and ethylbenzene-d_{10} (EB-d_{10}, Fig. S49ii†), were performed. KIE values (k_D, s^{-1}/k_H, s^{-1}) were observed to be 2.6 and 6.1 for $[\mathbf{IV,IV}]^{2+}$ with BA (0.15 M) and EB (0.20 M) and 43 for $[\mathbf{IV,IV\_1H}]^{3+}$ with BA (0.15 M)), which ensured that the HAA occurred and should probably be the rate determining step. The hydrogen tunnelling effect would contribute to the large KIE values.[5t] HAA would be achieved by a $1e^-$ transfer to the Ru(IV) center and for $[\mathbf{IV,IV}]^{2+}$, by one proton transfer to the terminal oxygen carbonato ligand to form $[\mathbf{III,IV\_1H}]^{2+}$. Then, one of the oxido ligands undergoes protonation that could originate from unavoidable water in solution to finally yield $[\mathbf{III,IV\_2H}]^{3+}$. With respect to $[\mathbf{IV,IV\_1H}]^{3+}$, one or both of the oxido ligand(s) function(s) as (a) proton acceptor(s) to form $[\mathbf{III,IV\_2H}]^{3+}$ or $\{[\mathbf{III,IV\_3H}]^{4+}\}^*$, respectively. The higher oxidation potential of $[\mathbf{IV,IV\_1H}]^{3+}$ compared to that of $[\mathbf{IV,IV}]^{2+}$ results in greater BDE_{C-H}; however, the basicity of carbonato oxygen may have an advantage, which may lead to a higher reaction rate. The analyses of the reaction products and reaction mechanisms including oxygen sources and oxygenation processes or product selectivity are underway.

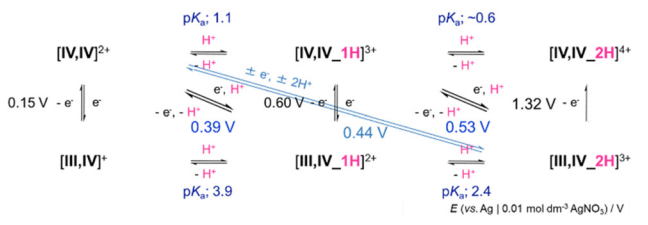

Scheme 2 Summary of pK_a values and redox potentials (*vs.* Ag|0.01 M $AgNO_3$).

Experimental

Syntheses and characterization of the complexes

All of the chemical reagents were used as purchased without further purification.

Syntheses of diruthenium complexes. *Caution!* Perchlorate salts and perchloric acid are potentially explosive and should be handled with care.

Ethylbis(2-pyridylmethyl)amine (ebpma) was prepared by a procedure given in ref. 8*a*. $[\{Ru^{III,IV}Cl_2(ebpma)\}_2(\mu\text{-}O)]PF_6\cdot(CH_3)_2CO$ was synthesized by a previously reported procedure[8c] from *fac*-$[Ru^{III}Cl_3(ebpma)]$[8a] *via* a triply chlorido-bridged diruthenium(II) complex, $[\{Ru^{II,II}(ebpma)\}_2(\mu\text{-}Cl)_3]PF_6$.[8b] $Na[\{Ru^{III,IV}(ebpma)\}_2(\mu\text{-}O)_2(\mu\text{-}O_2CO)]_2(PF_6)_3\cdot 7H_2O$ (Na[**III,IV**]$_2(PF_6)_3\cdot 7H_2O$) $[\{Ru^{III,IV}(ebpma)\}_2(\mu\text{-}O)_2(\mu\text{-}O_2COH)](PF_6)_2\cdot 1.5H_2O$ ([**III,IV_1H**]$(PF_6)_2\cdot 1.5H_2O$) were prepared according to the procedures reported in ref. 8*e*.

Synthesis of $[\{Ru^{III,IV}Cl_2(ebpma)\}_2(\mu\text{-}O)]ClO_4\cdot 0.75(CH_3)_2CO$. $[\{Ru^{III,IV}Cl_2(ebpma)\}_2(\mu\text{-}O)]ClO_4\cdot 0.75(CH_3)_2CO$ was synthesized in a similar manner to that of $[\{Ru^{III,IV}Cl_2(ebpma)\}_2(\mu\text{-}O)]PF_6\cdot(CH_3)_2CO$[8b] using $NaClO_4$ as a precipitate instead of NH_4PF_6. Yield: 62%. E. A./% calcd for $C_{30.25}H_{38.5}N_6O_{5.75}$

Cl_5Ru_2; calcd C, 37.94; H, 4.02; N, 8.78; found; C, 37.88; H, 4.04; N, 8.77%. IR spectrum (KBr disk); $\nu(ClO_4)$; 1092 cm^{-1}.

Synthesis of Na[{$Ru^{III,IV}$(ebpma)}$_2$(μ-O)$_2$(μ-O_2CO)]$_2$(ClO_4)$_3$·17H_2O (Na[III,IV]$_2$(ClO_4)$_3$·17H_2O). Na[{$Ru^{III,IV}$(ebpma)}$_2$(μ-O)$_2$(μ-O_2CO)]$_2$(ClO_4)$_3$·17H_2O was obtained in a similar manner to that of Na[**III,IV**]$_2$(PF_6)$_3$·7H_2O[8e] by using [{$Ru^{III,IV}Cl_2$(ebpma)}$_2$(μ-O)]ClO_4·0.75$(CH_3)_2CO$ as a starting material and $NaClO_4$ as a precipitating reagent. Yield; 38%. E. A./% calcd for $C_{58}H_{102}N_{12}O_{39}NaCl_3Ru_4$; calcd C, 32.69; H, 4.66; N, 7.73; found; C, 32.78; H, 4.80; N, 7.73%. IR spectrum (KBr disk); ν_{as}(CO); 1508(s), 1483(s), $\nu(ClO_4)$; 1087, 1116, 1144 cm^{-1}.

Synthesis of [{$Ru^{IV,IV}$(ebpma)}$_2$(μ-O)$_2$(μ-O_2CO)](X)$_2$·*n*H_2O ([IV,IV](X)$_2$·*n*H_2O)

X = ClO$_4$, n = 2. [**IV,IV**](ClO_4)$_2$·2H_2O was synthesized by a reaction of Na[**III,IV**]$_2$(ClO_4)$_3$·17H_2O[8e] (100 mg, 0.094 mmol) in an aqueous solution containing $(NH_4)_4[Ce^{IV}(SO_4)_4]$·2$H_2O$ (67 mg, 0.106 mmol) at pH 2.8. The volume of the obtained dark blue–green solution was reduced to less than 1 cm^3 by a slow evaporation under air, yielding brown single crystals. Yield; 50 mg, 52%. E. A./% calcd for $C_{29}H_{39}N_6O_{23}Cl_2Ru_2$ ([{Ru^{IV}(ebpma)}$_2$(μ-O)$_2$(μ-O_2CO)](ClO_4)$_2$·2H_2O); C, 34.78; H, 3.99; N, 8.39; found; C, 34.56; H, 3.76; N, 8.37%. FAB MS (+) (relative intensity, *m*/*z* ([M]$^{2+}$ = [{$Ru^{IV,IV}$(ebpma)}$_2$(μ-O)$_2$(μ-O_2CO)]$^{2+}$); 375.2 (33%, [M]$^{2+}$/2), 850.4 (100%, [M]$^{2+}$ + ClO_4^-). IR spectrum (KBr disk); ν_{as}(CO); 1570(sh), $\nu(ClO_4)$; 1078, 1109, 1123 cm^{-1}.

X = PF$_6$, n = 1.5. The PF_6–salt, [{$Ru^{IV,IV}$(ebpma)}$_2$(μ-O)$_2$(μ-O_2CO)](PF_6)$_2$·1.5H_2O, was synthesized in a similar manner to that of [**IV,IV**](ClO_4)$_2$·2H_2O by using Na[**III,IV**]$_2$(PF_6)$_3$·7H_2O[8e] as a starting material. E. A./% calcd for $C_{29}H_{37}N_6O_{6.5}Ru_2P_2F_{12}$; calcd C, 32.67; H, 3.47; N, 7.88; found; C, 32.57; H, 3.27; N, 7.92%. IR spectrum (KBr disk); ν_{as}(CO); 1591(sh), 1612 (s), 1635 (sh) cm^{-1}, $\nu_{as}(PF_6)$; 839 cm^{-1}. Λ_M = 214 S cm^2 mol^{-1} (1.0 mM).

Synthesis of [{$Ru^{IV,IV}$(ebpma)}$_2$(μ-O)$_2$(μ-O_2COH)](ClO_4)$_3$·HClO_4·7H_2O ([IV,IV_1H](ClO_4)$_3$·HClO_4·7H_2O). [**IV,IV_1H**](ClO_4)$_3$·HClO_4·7H_2O was obtained in a pH 1.16 HClO_4(aq.) solution of Na[**III,IV**]$_2$(ClO_4)$_3$·17H_2O[8e] (24 mg, 0.023 mmol) containing $(NH_4)_4[Ce^{IV}(SO_4)_4]$·2$H_2O$ (16 mg, 0.025 mmol) as an oxidant *via* the formation of [**IV,IV**]$^{2+}$. The volume of the obtained dark blue solution was reduced to less than 1 cm^3 by a slow evaporation under air, yielding dark blue–green single crystals. Yield; 20 mg, 89%. E. A./% calcd For $C_{29}H_{50}N_6O_{28}Cl_4Ru_2$ ([{$Ru^{IV,IV}$(ebpma)}$_2$(μ-O)$_2$(μ-O_2COH)](ClO_4)$_3$·HClO_4·7H_2O); C, 27.32; H, 3.92; N, 6.60; found; C, 27.03; H, 3.87; N, 6.82%. FAB MS (+) (relative intensity, *m*/*z* ([M]$^{3+}$ = [{$Ru^{IV,IV}$(ebpma)}$_2$(μ-O)$_2$(μ-O_2COH)]$^{3+}$); 951.3 (11%, {[M]$^{3+}$ + 2ClO_4^-}$^+$). IR spectrum (KBr disk); ν_{as}(CO); 1437(sh), 1448(sh), $\nu(ClO_4)$; 1081, 1091, 1124 cm^{-1}. Λ_M = 601 S cm^2 mol^{-1} (1.0 mM).

Measurements

Elemental analyses were performed with a PerkinElmer Model 2400-II system or performed in the Institute of Physical and Chemical Research (RIKEN). Fast atom bombardment mass spectrometry (FAB MS) was performed with a JEOL Model JMS SX700 V system, using *m*-nitrobenzyl alcohol as a matrix. The effective magnetic moments, μ_{eff}/μ_B, were measured with a Sherwood Scientific Magway MSB MK1 balance at 298 K using $Hg[Co^{II}(SCN)_4]$ as a calibrant. X-band electron spin resonance (ESR) spectra were recorded with a JEOL Model JESFA300 ESR spectrometer at 93 K. IR spectra were recorded on a Shimadzu IR Model Affinity-1 spectrophotometer with 2.0 cm^{-1} resolution using the samples prepared as KBr disks. UV-vis-NIR spectra were measured on a Shimadzu UV-3600 Plus or 1900i in an organic solvent or in aqueous solution using a quartz cell of 1 cm path length. Cyclic voltammetry (CV) and Osteryoung square wave voltammetry (OSWV) were performed in CH_3CN containing 0.1 mol dm^{-3} tetra-*n*-butylammonium perchlorate (TBAP, Nakarai Tesque Ltd) as a supporting electrolyte with a platinum or a glassy carbon disk working electrode (ϕ = 1.6 mm), an Ag|0.01 mol dm^{-3} $AgNO_3$ reference electrode, and a platinum wire counter electrode using an ALS 630E electrochemical analyser. At the end of each measurement, ferrocene ($[Fe^{III}(Cp)_2]^+/[Fe^{II}(Cp)_2]$, 0.074 V *vs.* Ag| 0.01 mol dm^{-3} $AgNO_3$ (CH_3CN)) was added as an internal standard to tune the redox potentials. For the measurements in 0.1 mol dm^{-3} NaOH–HClO_4 aqueous solutions, a glassy carbon working electrode (ϕ = 1.0 mm), an Ag|AgCl 3.0 mol dm^{-3} NaCl reference electrode, and a platinum wire counter electrode were used. Hydrodynamic voltammetry (HDV) was performed with a rotating glassy carbon disk working electrode (ϕ = 3.0 mm) by a BAS RDE-2 rotating electrode.

X-ray crystallography

Single crystals suitable for X-ray diffraction were grown by slow evaporation of the pH 2.8 or 1.1 solution of [**IV,IV**](ClO_4)$_2$·2H_2O and [**IV,IV_1H**](ClO_4)$_3$·HClO_4·H_2O, respectively, at around 50 °C. The intensity data were collected on a Rigaku Model Synergy-S system, using multilayer mirror monochromated Cu*K*α radiation (1.54184 Å). All the calculations were performed using CrysAlis^{Pro} (Data Collection and Processing Software, Rigaku Corporation (2015)). Structures were solved by direct methods, expanded using Fourier techniques and refined using full-matrix least-squares techniques on F_2 using SHELXT with Olex2 1.2 (CCDC 2115482 for [**IV,IV**](ClO_4)$_2$·2H_2O and 2115484 for [**IV,IV_1H**](ClO_4)$_3$·HClO_4·H_2O).†

Reactions in organic solvents and in the presence of organic compounds

Superdehydrated solvents are of 99.8% grade. Deuterated purity for acetone-d_6 was 99.6%, for acetonitrile-d_3 99.8%, for benzylalcohol-d_2 99% and for ethylbenzene-d_{10} 99%. C–H oxidation reactions of organic compounds were studied in superdehydrated CH_3CN under air at 25 °C with complexes of 0.20 mM and substrates ranging from 0.05 M to 0.2 M.

DFT calculations

Density functional theory (DFT) calculations were performed using the Gaussian 09 program.[18] The geometrical optimizations were performed at the unrestricted B3LYP level of DFT, with Los Alamos effective core potential plus minimal basis (LANL2MB) or double-ζ (LANL2DZ) basis sets.

Conclusions

The Ru(IV)–Ru(IV) complexes with the $\{Ru_2(\mu\text{-}O)_2\}$ core and a bridging carbonato or hydrogencarbonato ligand, which are structurally analogous to the reaction centers of sMMO, in particular, the plausible intermediate Q having the "closed-core", were isolated and studied in detail. It should be emphasized that the carbonato or hydrogencarbonato ligand was stabilized in the Ru(IV)–Ru(IV) centers and they did not undergo decarboxylation even at as low as pH 0.5. The direct comparisons of spectroscopic properties and structural parameters with those of the Ru(III)–Ru(IV) species are worth noting since all the complexes are designed using the same tridentate ligand (ebpma). The electron transition energies on the $\{Ru_2(\mu\text{-}O)_2\}$ core were in relation to the electronic state of the Ru centers $[\mathbf{IV,IV}]^{2+}$ (λ_{max} = 760 nm) and $[\mathbf{IV,IV\_1H}]^{3+}$ (669 nm) *vs.* $[\mathbf{III,IV}]^{+}$ (1067 nm) and $[\mathbf{III,IV\_1H}]^{2+}$ (972 nm), and to the electrostatic nature of the bridging ligand, (O_2Y–Z). The structural parameters of the $\{Ru_2(\mu\text{-}O)_2\}$ diamond core changed due to the higher cationic character of the Ru(IV)–Ru(IV) centers compared to the Ru(III)–Ru(IV) ones. However, it was also true that the ebpma ligand seemed to play a nice role in minimizing the impact of the change in the electronic structure on the shape of the diamond core, $\{Ru_2(\mu\text{-}O)_2\}$.

Reactions in solvents and oxidation reactions of organic substrates using these Ru(IV)–Ru(IV) complexes were investigated in dehydrated acetonitrile, which was revealed to be the only solvent suitable for the reaction mediator for our system. The relationships between the reaction rate and the BDE of substrates, and the different reaction processes between $[\mathbf{IV,IV}]^{2+}$ and $[\mathbf{IV,IV\_1H}]^{3+}$ were found. Further investigations on the reaction products will be performed by analysing the reaction conditions in detail. This work would contribute to the strctural model of metalloenzymes and would also give insights into some model reactions of C–H activation.

Conflicts of interest

There are no conflicts to declare.

Acknowledgements

We appreciate Prof. Dr Shinkoh Nanbu for the theoretical calculations. This work was supported by JSPS KAKENHI Grant Number 22K14696.

References

1 (*a*) C. E. Tinberg and S. J. Lippard, *Acc. Chem. Res.*, 2011, **44**, 280; (*b*) R. Banerjee, Y. Proshlyakov, J. D. Lipscomb and D. A. Proshlyakov, *Nature*, 2015, **518**, 431.

2 (*a*) A. B. Jacobs, R. Banerjee, D. E. Deweese, A. Braun, J. T. Babicz Jr., L. B. Gee, K. D. Sutherlin, L. H. Böttger, Y. Yoda, M. Saito, S. Kitao, Y. Kobayashi, M. Seto, K. Tamasaku, J. D. Lipscomb, K. Park and E. I. Solomon, *J. Am. Chem. Soc.*, 2021, **143**, 16007; (*b*) G. Xue, R. D. Hont, E. Münck and L. Que Jr., *Nat. Chem.*, 2010, **2**, 400; (*c*) M. Martinho, G. Xue, A. T. Fiedler, L. Que Jr., E. L. Bominaar and E. Münck, *J. Am. Chem. Soc.*, 2009, **131**, 5823; E. Y. Tshuva and S. J. Lippard, *Chem. Rev.*, 2004, **104**, 987.

3 Y. Morimoto, Y. Takagi, T. Saito, T. Ohta, T. Ogura, N. Tohnai, M. Nakano and S. Itoh, *Angew. Chem., Int. Ed.*, 2018, **57**, 7640.

4 (*a*) R. Singh, G. Ganguly, S. O. Malinkin, S. Demeshko, F. Meyer, E. Nordlander and T. K. Paine, *Inorg. Chem.*, 2019, **54**, 1862 and the references therein; (*b*) S. T. Kleespies, W. N. Oloo, A. Mukherjee and L. Que Jr., *Inorg. Chem.*, 2015, **54**, 5053 and the references therein; (*c*) D. Wang, M. Zhang, P. Bühlmann and L. Que Jr., *J. Am. Chem. Soc.*, 2010, **132**, 7638; (*d*) C. R. Goldsmith and T. D. P. Stack, *Inorg. Chem.*, 2006, **45**, 6048; (*e*) J. Kaizer, E. J. Klinker, N. Y. Oh, J.-U. Rohde, W. J. Song, A. Stubna, J. Kim, E. Münck, W. Nam and L. Que Jr., *J. Am. Chem. Soc.*, 2004, **126**, 472; (*f*) C. R. Goldsmith, R. T. Jonas and T. D. P. Stack, *J. Am. Chem. Soc.*, 2002, **124**, 83.

5 (*a*) H. Kotani, H. Shimomura, K. Ikeda, T. Ishizuka, Y. Shiota, K. Yoshizawa and T. Kojima, *J. Am. Chem. Soc.*, 2020, **142**, 16982; (*b*) H. Kotani, H. Shimomura, M. Horimoto, T. Ishizuka, Y. Shiota, K. Yoshizawa, S. Yanagisawa, Y. Kawahara-Nakagawa, M. Kubo and T. Kojima, *Dalton Trans.*, 2019, **48**, 13154; (*c*) C.-W. Tse, Y. Liu, T. W.-S. Chow, C. Ma, W.-P. Yip, X.-Y. Chang, K.-H. Low, J.-S. Huang and C.-M. Che, *Chem. Sci.*, 2018, **9**, 2803; (*d*) R. Ray, S. Chandra, D. Maiti and G. K. Lahiri, *Chem. – Eur. J.*, 2016, **22**, 8814; (*e*) T. Ishizuka, H. Kotani and T. Kojima, *Dalton Trans.*, 2016, **45**, 16727; (*f*) S. N. Dhuri, Y.-M. Lee, M. S. Seo, J. Cho, D. D. Narulkar, S. Fukuzumi and W. Nam, *Dalton Trans.*, 2015, **44**, 7634; (*g*) S. N. Dhuri, K.-B. Cho, Y.-M. Lee, S. Y. Shin, J. H. Kim, D. Mandal, S. Shaik and W. Nam, *J. Am. Chem. Soc.*, 2015, **137**, 8623; (*h*) T. Ishizuka, S. Ohzu and T. Kojima, *Synlett*, 2014, **25**, 1667; (*i*) T. Kojima, K. Nakayama, K. Ikemura, T. Ogura and S. Fukuzumi, *J. Am. Chem. Soc.*, 2011, **133**, 11692; (*j*) Y. Hirai, T. Kojima, Y. Mizutani, Y. Shiota, K. Yoshizawa and S. Fukuzumi, *Angew. Chem., Int. Ed.*, 2008, **47**, 5772; (*k*) C.-M. Che, J.-L. Zhang, R. Zhang, J.-S. Huang, T.-S. Lai, W.-M. Tsui, X.-G. Zhou, Z.-Y. Zhou, N. Zhu and C. K. Chang, *Chem. – Eur. J.*, 2005, **11**, 7040; (*l*) R. Zhang, W.-Y. Yu and C.-M. Che, *Tetrahedron: Asymmetry*, 2005, **16**, 3520; (*m*) W. K. Seok and T. J. Meyer, *Inorg. Chem.*, 2005, **44**, 3931; (*n*) T. J. Meyer, *Inorg. Chem.*, 2005, **44**, 2150; (*o*) J. R. Bryant and J. M. Mayer, *J. Am. Chem. Soc.*, 2003, **125**, 10351; (*p*) W. W. Y. Lam, S.-M. Yiu, D. T. Y. Yiu, T.-C. Lau, W.-P. Yip and C.-M. Che, *Inorg. Chem.*, 2003, **42**, 8011; (*q*) S. Funyu, T. Isobe, S. Takagi, D. A. Tryk and H. Inoue, *J. Am. Chem. Soc.*, 2003, **125**, 5734; (*r*) D. T. Y. Yiu, M. F. W. Lee, W. W. Y. Lam and T.-C. Lau, *Inorg. Chem.*, 2003, **42**, 1225; (*s*) C.-M. Che, K.-W. Cheng, M. C. W. Chan, T.-C. Lau and C.-K. Mak, *J. Org. Chem.*, 2000, **65**, 7996; (*t*) W.-C. Cheng, W.-Y. Yu, C.-K. Li and C.-M. Che, *J. Org.*

Chem., 1995, **60**, 6840; (*u*) C.-M. Che, V. Q.-Q. Yam and T. C. W. Mak, *J. Am. Chem. Soc.*, 1990, **112**, 2284; (*v*) J. C. Dobson and T. J. Meyer, *Inorg. Chem.*, 1988, **27**, 3283.

6 (*a*) T. Fujimoto, Y. Hirata, H. Sugimoto, M. Miyanishi, Y. Shiota, K. Yoshizawa and S. Itoh, *Dalton Trans.*, 2022, **51**, 1123; (*b*) T. Fujimoto, Y. Hirata, H. Sugimoto, M. Miyanishi, Y. Shiota, K. Yoshizawa and S. Itoh, *Bull. Chem. Soc. Jpn.*, 2022, **95**, 64; (*c*) D. M. E. van Niekerk, T. E. Geswindt and W. J. Gerber, *Inorg. Chem.*, 2021, **60**, 782; (*d*) T.-C. Lau, *Angew. Chem., Int. Ed.*, 2016, **55**, 288; (*e*) Y. Liu, S.-M. Ng, W. W. Y. Lam, S.-M. Yiu and T.-C. Lau, *J. Am. Chem. Soc.*, 2004, **126**, 14921.

7 T. Nakano, T. Abe, T. Matsumoto, K. Kimura, G. Nakamura, S. Hayami, Y. Shiota, K. Yoshizawa and S. Ogo, *RSC Adv.*, 2022, **12**, 1253.

8 (*a*) Y. Shimizu, S. Fukui, T. Oi and H. Nagao, *Bull. Chem. Soc. Jpn.*, 2008, **81**, 1285; (*b*) T. Suzuki, K. Matsuya, T. Kawamoto and H. Nagao, *Eur. J. Inorg. Chem.*, 2014, 722; (*c*) T. Suzuki, Y. Suzuki, T. Kawamoto, R. Miyamoto, S. Nanbu and H. Nagao, *Inorg. Chem.*, 2016, **55**, 6830; (*d*) T. Misawa-Suzuki, T. Watanabe, M. Okamura, S. Nanbu and H. Nagao, *Inorg. Chem.*, 2020, **59**, 612; (*e*) T. Misawa-Suzuki, S. Mafune and H. Nagao, *Inorg. Chem.*, 2021, **60**, 9996.

9 K. J. Jonasson, A. H. Mousa and O. F. Wendt, *Polyhedron*, 2018, **143**, 132.

10 A. Looney, R. Han, K. McNeill and G. Parkin, *J. Am. Chem. Soc.*, 1993, **115**, 4690.

11 F. Bottomley and J. Chen, *Organometallics*, 1992, **11**, 3404.

12 T. Ghatak, A. Sinha, S. M. W. Rahaman and J. K. Bera, *Inorg. Chim. Acta*, 2011, **372**, 94.

13 N. J. Meanwell, A. J. Smith, H. Adams, S. Okeya and P. M. Maitlis, *Organometallics*, 1983, **2**, 1705.

14 (*a*) S. K. Tyrlik, M. Kisielinska and J. C. Huffman, *Transition Met. Chem.*, 1995, **20**, 413; (*b*) M. Orts-Arroyo, I. Castro, F. Llobet and J. Martínez-Lillo, *Cryst. Growth Des.*, 2020, **20**, 2044.

15 (*a*) J. M. Power, K. Evertz, L. Henling, R. Marsh, W. P. Schaefer, J. A. Labinger and J. E. Bercaw, *Inorg. Chem.*, 1990, **29**, 5058; (*b*) E. P. Kelson, L. M. Healing, W. P. Schaefer, J. A. Labinger and J. E. Bercaw, *Inorg. Chem.*, 1993, **32**, 2863.

16 P. Neubold, S. P. C. D. Vedova, B. K. Wieghardt, B. Number and J. Weiss, *Angew. Chem., Int. Ed. Engl.*, 1989, **28**, 763.

17 A. Geilenkirchen, P. Neubold, R. Schneider, K. Wieghardt, U. Florke, H.-J. Haupt and B. Nuber, *J. Chem. Soc., Dalton Trans.*, 1994, 457.

18 M. J. Frisch, G. W. Trucks, H. B. Schlegel, G. E. Scuseria, M. A. Robb, J. R. Cheeseman, G. Scalmani, V. Barone, B. Mennucci, G. A. Petersson, H. Nakatsuji, M. Caricato, X. Li, H. P. Hratchian, A. F. Izmaylov, J. Bloino, G. Zheng, J. L. Sonnenberg, M. Hada, M. Ehara, K. Toyota, R. Fukuda, J. Hasegawa, M. Ishida, T. Nakajima, Y. Honda, O. Kitao, H. Nakai, T. Vreven, J. A. Montgomery, J. E. Peralta, F. Ogliaro, M. Bearpark, J. J. Heyd, E. Brothers, K. N. Kudin, V. N. Staroverov, R. Kobayashi, J. Normand, K. Raghavachari, A. Rendell, J. C. Burant, S. S. Iyengar, J. Tomasi, M. Cossi, N. Rega, J. M. Millam, M. Klene, J. E. Knox, J. B. Cross, V. Bakken, C. Adamo, J. Jaramillo, R. Gomperts, R. E. Stratmann, O. Yazyev, A. J. Austin, R. Cammi, C. Pomelli, J. W. Ochterski, R. L. Martin, K. Morokuma, V. G. Zakrzewski, G. A. Voth, P. Salvador, J. J. Dannenberg, S. Dapprich, A. D. Daniels, Ö. Farkas, J. B. Foresman, J. V. Ortiz, J. Cioslowski and D. J. Fox, *Gaussian 09, Revision B.01*, Gaussian, Inc., Wallingford, CT, 2009.

19 Y.-R. Luo, *Comprehensive Handbook of Chemical Bond Energies*, CRC, Boca Raton, FL, 2007.

20 J. J. Warren, T. A. Tronic and J. M. Mayer, *Chem. Rev.*, 2010, **110**, 6961.

21 (*a*) J. R. Murdoch, *J. Am. Chem. Soc.*, 1972, **94**, 4410; (*b*) J. E. Leffler, *Science*, 1953, **117**, 340.